GEOMATICS AND ENVIRONMENTAL ENGINEERING • Volume 15 • Number 2 • 2021

https://doi.org/10.7494/geom.2021.15.2.5

Bambang Bakri[1], Khaeryna Adam[2], Amran Rahim[3]

# Spatio-Temporal Model of Extreme Rainfall Data in the Province of South Sulawesi for a Flood Early Warning System

**Abstract:** In this study, we model extreme rainfall to study the high rainfall events in the province of South Sulawesi, Indonesia. We investigated the effect of the El Nino South Oscillation (ENSO), Indian Ocean Dipole Mode (IOD), and Madden–Julian Oscillation (MJO) on extreme rainfall events. We also assume that events in a location are affected by events in other nearby locations. Using rainfall data from the province of South Sulawesi, the results showed that extreme rainfall events are related to IOD and MJO.

**Keywords:** spatio-temporal model, extreme rainfall, province of South Sulawesi, El Nino South Oscillation, Indian Ocean Dipole Mode, and Madden–Julian Oscillation

Received: 18 September 2020; accepted: 19 November 2020



[1] Hasanuddin University, Faculty of Technic, Department of Civil Engineering, Makassar, Indonesia, email: bambangbakri@gmail.com, ORCID ID: https://orcid.org/0000-0001-9006-2018

[2] Hasanuddin University, Faculty of Mathematics and Natural Sciences, Department of Mathematics, Makassar, Indonesia, email: ririn.adam@gmail.com

[3] Hasanuddin University, Department of Mathematics, Faculty of Mathematics and Natural Sciences, Makassar, Indonesia, email: amran@science.unhas.ac.id (corresponding author), ORCID ID: https://orcid.org/0000-0002-9832-8738

## 1. Introduction

Extreme rainfall has a detrimental effect on human life and the environment. Extreme rainfall is that which rarely occurs in a location within a certain time [1]. There are two approaches used in determining extreme rainfall, namely Peak Over Threshold (POT) and Block Maxima (BM) [2]. In the POT approach, extreme rainfall is expressed as rainfall that is greater than the threshold value. Meanwhile, in the BM approach, extreme rainfall is expressed as the maximum value in a block of time.

Extreme rainfall can be divided into high extreme rainfall and low extreme rainfall. High rainfall is associated with floods or landslides, while low rainfall is associated with drought. Both types of extreme rainfall have adverse effects on human life and the environment. High extreme rainfall is defined as rainfall that is more than or equal to the $75^{th}$ or $90^{th}$ percentile [1, 3].

Extreme rainfall in Indonesia is strongly linked to the phenomena of global climate change such as the El Nino South Oscillation (ENSO) [4], Indian Ocean Dipole Mode (IOD) [5], and Madden–Julian Oscillation (MJO) [6]. This is because Indonesia is one of the tropical regions between the Pacific Ocean and the Indian Ocean and the continents of Asia and Australia. This study aims to model the rate of extreme rainfall events related to the effects of climate change on 21 areas in the province of South Sulawesi in order to construct an early warning system.

The number of extreme rainfall events is a counting process that can be modeled into the Poisson model [7]. The Poisson processes with constant intensity are called Homogeneous Poisson processes, while Poisson processes with time-dependent intensities are called non-homogeneous Poisson processes (NHPP). The number of extreme rainfall events over time certainly varies because of climate change, in other words they are not constant. Thus, non-homogeneous Poisson processes characterized by time-dependent intensity functions are realistic enough to be applied when modeling extreme rainfall phenomena.

The NHPP model has been applied in various disciplines, for example modeling the arrival rate of containers in port operations and management [8], analyzing ozone behavior [9], analyzing rainfall occurrence [10], and modeling the frequency of extreme rainfall [11]. However, the studies that have been carried out are mostly focused on the development of time-dependent models, whilst extreme rainfall modeling involves data that is observed at different times and locations so that often observations in a location are affected by observations in other nearby locations. Thus, the addition of spatial effects to a model should be considered.

Some researchers add spatial effects to their research model to explain the possible correlations and sources of variance that are not explained in the model. Huang et al. [12] applied Conditional Auto-Regressive (CAR) to explain spatial correlation in modeling $N_2O$ emissions. Rusworth et al. [13] present a new model for estimating the effects of air pollution on human health by using the spatial

effect of CAR on Spatio-temporal model. Sharkey and Winter [14] add the spatial effect of CAR distribution on the Generalized Pareto Distribution (GPD) parameter for precipitation modeling. Marco et al. [15] use CAR as a spatial effect in his research on modeling drug crime. The addition of the spatial effect of CAR on the models of these studies was constructed using the Bayesian hierarchy framework. A Bayesian hierarchy is considered a flexible framework and allows the incorporation of various sources of uncertainty [14].

## 2. Data

The data used in this study are daily rainfall data at 60 locations in 21 areas in the province of South Sulawesi obtained from the Global Satellite Mapping of Precipitation or GSMaP (ftp://hokusai.eorc.jaxa.jp). This research analyses extreme rainfall events for 8 years from 2009 to 2016. Three important climatic factors: the El Nino Southern Oscillation (ENSO), the Indian Ocean Dipole (IOD), and the Madden–Julian Oscillation (MJO) are considered in this study to understand their effects on extreme rainfall occurrence. ENSO and IOD data were obtained from the National Oceanic and Atmospheric (NOAA) and MJO data from the Bureau of Meteorology. Figure 1 shows the districts in the province of South Sulawesi, Indonesia and rainfall station locations.

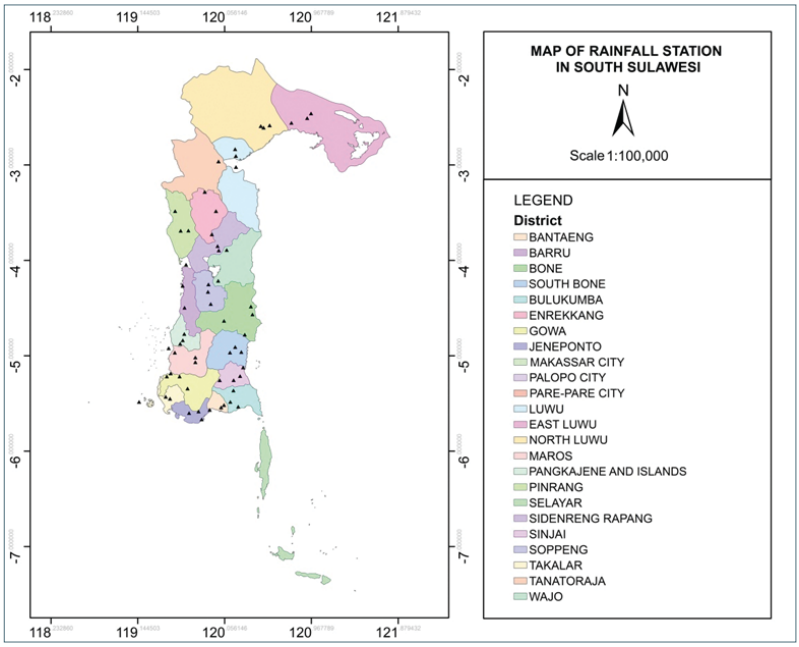


**Fig. 1.** Map of rainfall station locations in the province of South Sulawesi

## 3. Methodology

The steps in this study are as follows: Collecting data, determine extreme rainfall data by calculating the 75th percentile value in a day's rainfall, counting the number of days with rainfall more than or equal to the 75th percentile (D75) every month, identify spatial correlations with Moran's I test, construct NHPP models for the number of extreme rainfall events D75 with three independent variables with the addition of spatial effects of CAR in the Bayesian Hierarchy framework, parameter estimation using WinBugs Version 3.0.2 software, and interpretation of research results.

## 4. Extreme Rainfall Modeling

Modeling the rate of extreme rainfall events is carried out within the Hierarchical Bayesian framework. Non-homogeneous Poisson modeling with spatial effects using the Bayesian hierarchy method consists of three steps, namely the data modeling step, the process modeling step, and the prior distribution selection step. The hierarchical modeling structure is described as follows:

Let $y_{ti}$ denotes the number of extreme rainfall day in time $t$, $t = 1, 2, ..., T$ and area $i$, $i = 1, 2, ..., n$. $y_{ti}$ is Poisson distribution data, which can be shown through the Kolmogorov–Smirnov test. $y_{ti}$ is modeled as Poisson distribution data with the parameter $\lambda_{ti}$, then the data modeling step can be written as follows:

$$y_{ti} \sim Poisson(\lambda_{ti}),$$

where $\lambda_{ti}$ depends on the time $t$ and the location $i$ of the event with the likelihood function as follows:

$$L(\theta) = f(\mathbf{Y} \mid \boldsymbol{\lambda}) = \prod_{t=1}^{T} \prod_{i=1}^{n} \frac{\lambda_{ti}^{y_{ti}} e^{-\lambda_{ti}}}{y_{ti}!}.$$

In process modeling, it is assumed that the rate of extreme rainfall events $\lambda_{ti}$ is based on spatial processes since neighboring locations have more similar characteristics than locations farther away, so that $u_i$ as spatial random effects are added to the model. Also, three climate covariates that are thought to affect extreme rainfall events: MJO, IOD, and ENSO are also included in the model thus the model can be written as follows:

$$\log \lambda_{ti} = \beta_0 + \beta_1 MJO_{ti} + \beta_2 NINO_{ti} + \beta_3 IOD_{ti} + u_i,$$

where $\beta_0$ is global intercept, $\beta_1$, $\beta_2$, $\beta_3$ are regression coefficients, $MJO_{ti}$, $NINO_{ti}$, $IOD_{ti}$ are predictors at time $t$ in location $i$ and $u_i$ are spatial random components at location $i$ modeled with priors conditional autoregressive (CAR) distribution.

The use of a log-link in parameter estimation aims to ensure the parameter value is a non-negative number. Banerjee et al. [16] in Sharkey and Winter [14] write the CAR model with conditional prior for $u_i$ as:

$$u_i \mid u_{-i} \sim N\left(\sum_{j\in n}\frac{u_{-i}}{w_{i+}}, \frac{\tau^2}{w_{i+}}\right),$$

where $u_i$ is spatial random effect, $\tau^2$ is the variance, $w_{i+} = \sum_{j=1}^{n} w_{ij}$ with $w_{i+}$ is the number of neighbors of cell location $i$, $w_{ij}$ is spatial weight on the spatial weight matrix $\boldsymbol{W}$. A real $n \times n$ matrix defining spatial proximity between cells $i$ and $j$ with $w_{ij} = 1$ if location $i$ and $j$ are adjacent and $w_{ij} = 0$ otherwise.

The last step in hierarchical modeling is defining priors and assumed that the parameters at each step of the model are independent. Assuming there is no prior knowledge of one of the parameters in the model, it is chosen to set non-informative prior for $\beta_k = (\beta_0, \beta_1, \beta_2, \beta_3)$ with consideration of $\beta_k \sim N(\mu, \varphi)$ where hyperprior $\mu$ and $\varphi$ are normally distributed with mean-centered on zero and a large and fixed variant [14]. The definition of the prior is described as follows: Parameter $\beta_k = \{\beta_0, \beta_1, \beta_2, \beta_3\}$ are priors with Normal distribution, $\beta_k \sim N(\mu, \varphi)$, $\mu \sim N(0, 100)$, $\varphi \sim N(0, 100)$, $\tau \sim Gamma(0.5, 0.0005)$.

Proportionally, the posterior distribution is the product of the likelihood function with prior. The parameters that will be estimated are written as:

$$\boldsymbol{\theta} = \{\beta_0, \beta_1, \beta_2, \beta_3, u_i\}$$

with hyperparameter:

$$\boldsymbol{\psi} = \{\mu, \varphi, \tau\},$$

thus the likelihood function in this model is:

$$f(\boldsymbol{y} \mid \beta_0, \beta_1, \beta_2, \beta_3, u_i, \mu, \varphi, \tau) = \prod_{t=1}^{T}\prod_{i=1}^{n} f(y_{ti} \mid \beta_0, \beta_1, \beta_2, \beta_3, u_i, \mu, \varphi, \tau).$$

Therefore, the posterior distribution can be written as follows.

$$f(\boldsymbol{\theta}, \boldsymbol{\psi} \mid \boldsymbol{y}) = f(\boldsymbol{y} \mid \boldsymbol{\theta}, \boldsymbol{\psi}) \times f(\boldsymbol{\theta} \mid \boldsymbol{\psi}) \times f(\boldsymbol{\psi}),$$
$$f(\boldsymbol{\theta}, \boldsymbol{\psi} \mid \boldsymbol{y}) = f(y_{ti} \mid \beta_0, \beta_1, \beta_2, \beta_3, u_i, \mu, \varphi, \tau) \times f(\beta_0 \mid \mu, \varphi) \times f(\beta_1 \mid \mu, \varphi) \times$$
$$\times f(\beta_2 \mid \mu, \varphi) \times f(\beta_3 \mid \mu, \varphi) \times f(u_i \mid \tau) \times f(\varphi) \times f(\tau).$$

Model parameters are estimated by means of the Bayes method using the Markov Chain Monte Carlo (MCMC) algorithm with WinBugs version 3.0.2 software.

## 5. Result

The parameter estimation results with the Bayesian method are good when the estimated parameters converge. The convergence of the estimation results was observed by the visual inspection of trace samples for each chain, density, history, autocorrelation, and convergence statistics of Gelman-Rubin. The estimation results for the high extreme rainfall rate models are obtained by carrying out an MCMC run of 10.000 iterations with 1.000 burn-in period. Trace sample plots for each chain, density, history, autocorrelation, and convergence statistics of Gelman–Rubin show that MCMC is mixing well.

The estimation results for the number of extreme rainfall days (D75) model are presented in Table 1. The first column in each Table is the covariate parameter (factors) that are thought to affect extreme rainfall events rate, the mean column shows the magnitude of the model parameter value, and for the next three columns, namely val2.5% (credible lower limit interval), median, and val97.5% (upper limit of the credible interval) is the estimated value on the 95% credible interval. Covariates with values at credible intervals that do not contain zero value are considered to significantly affect the rate of the number of extreme rainfall days.

**Table 1.** Parameter posterior estimation results for the rate of D75 model

| Parameter | Mean | Standard deviation | Val2.5% | Median | Val97.5% |
|---|---|---|---|---|---|
| $\beta_0$ | 0.6365 | 0.0563 | 0.5274 | 0.6368 | 0.7469 |
| $\beta_1$ | 0.1864 | 0.0566 | 0.0749 | 0.1863 | 0.2972 |
| $\beta_2$ | −0.0005 | 0.0181 | −0.0367 | −0.0007 | 0.0349 |
| $\beta_3$ | −0.7952 | 0.0645 | −0.9203 | −0.7945 | −0.6697 |
| $\tau$ | 11.9300 | 5.5690 | 4.5500 | 10.7900 | 25.7800 |

Based on the estimation results in Table 1, what is stated to affect the rate of D75 in South Sulawesi with a confidence interval of 95% is MJO and IOD. This can be seen from the results of estimating the parameters $\beta_1$ and $\beta_3$ whose values do not contain zero on the credible interval. In contrast to ENSO, since it contains zero on the credible interval on the results of the $\beta_2$ parameter estpmation, it stated that ENSO did not show a significant result for D75 in the province of South Sulawesi for a period of 2009 to 2016. Meanwhile, the CAR parameter ($\tau$) shows that there is a spatial dependency between neighboring locations of events.

The rate of the number of extreme rainfall days in the province of South Sulawesi can be modeled as follows:

$$\log \lambda_{ti}^{D75} = 0.6365 + 0.1864 MJO_{ti} - 0.7952 IOD_{ti}.$$

From the estimation results for D75 rates, it stated that for D75 behavior towards the climate covariate. The MJO and the IOD significantly influence while ENSO does not affect significantly. The CAR parameter (τ) significantly affects both the MJO and the IOD. It means that in the case of extreme rainfall events there are spatial dependencies in neighboring locations.

The description of D75 in the province of South Sulawesi (see Fig. 2) shows a pattern that varies over time. The presence of spatial dependencies occurred in the province of South Sulawesi. Several locations have similar colors.

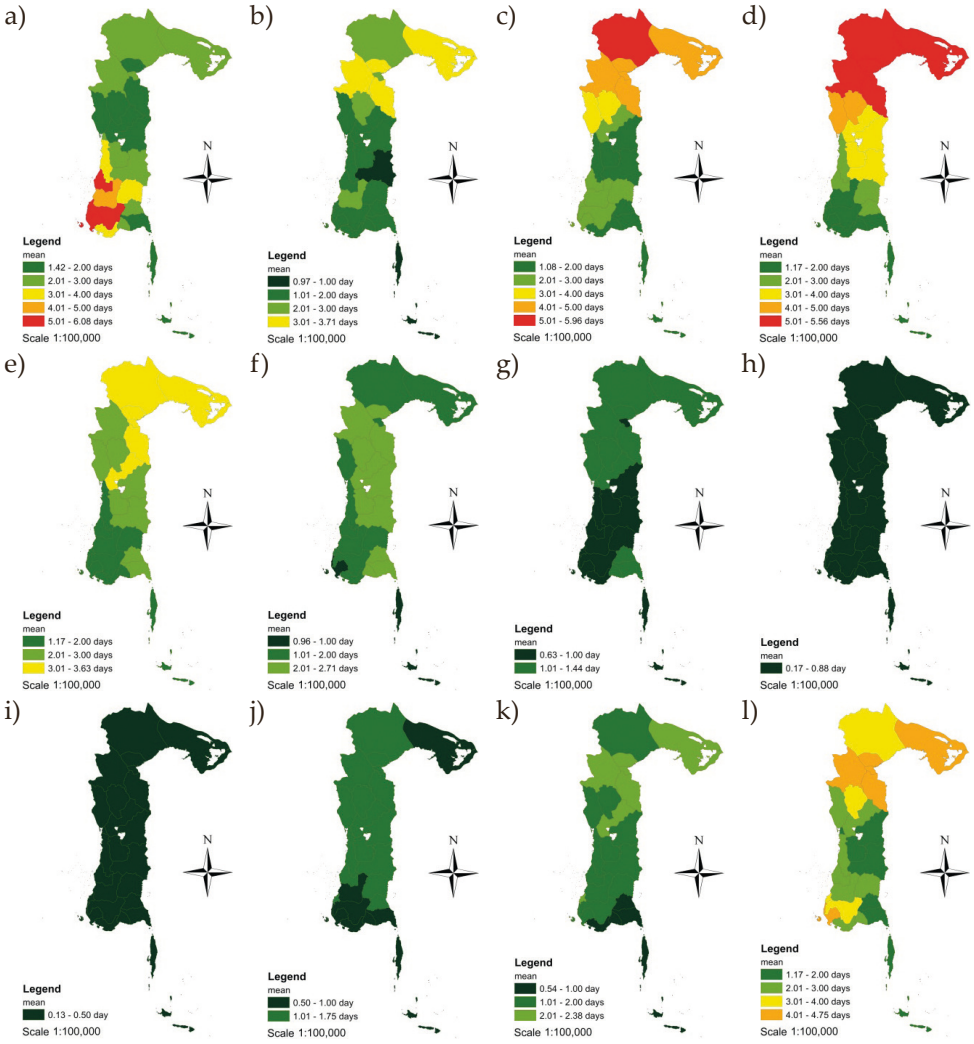


**Fig. 2.** Map of the high extreme rainfall rate in the period 2009 to 2016: a) January, b) February, c) March, d) April, e) May, f) June, g) July, h) August, i) September, j) October, k) November, l) December

The rate of D75 in the province of South Sulawesi in the period 2009 to 2016 ranges from one to six days (see Fig. 2). The maximum rate of extreme rainfall days in six days and this occurs in January and April, with the rate of D75 in one-day for August and September. The variation in the rate of occurrence is certainly related to the geography and topography at the scene. Although globally the rate of extreme rainfall events is significantly affected by MJO and IOD, extreme rainfall events in several locations in South Sulawesi are influenced by the local nature of the location.

## 6. Discussion

The modeling of extreme rainfall events rate in this study was carried out by considering three climate covariates that were thought to affect extreme rainfall events: ENSO [4], IOD [5], and MJO [6]. Climate change that changes from time to time causes the incidence of extreme rainfall is not constant or changes over time. In that case, the NHPP is quite realistic to be used to model the rate of D75 that depend on changes in time.

Globally, 21 areas of observation in the province of South Sulawesi have spatial correlations with the location of their neighbors. This can be seen from the Moran index value $I = 0.2990$. Thus the addition of spatial effects to rainfall modeling was carried out to explain the spatial random effects as carried out by [14]. Spatial dependence is done by selecting prior CAR on spatial random effects. In this study, prior CAR in the NHPP model is used to model high extreme rainfall events in the province of South Sulawesi.

The effect of the global climate on the rate of the number of extreme rainfall days is shown in Table 1. Both MJO and IOD showed a significant effect on the number of extreme rainfall days in the province of South Sulawesi. This can be seen from the results of estimating the parameters $\beta_1$ and $\beta_3$ whose values do not contain zero on the credible interval. This is in contrast to ENSO, because it contains zero on the credible interval on the results of the $\beta_2$ parameter estimation. ENSO has no significant effect on the rate of D75 in the province of South Sulawesi for the period of 2009 to 2016.

In general, ENSO has a varied influence on rainfall intensity and the number of rainy days both spatially and temporally. According to Deni et al. [17], ENSO has a major effect on rainfall anomalies in Indonesia. In the east of Indonesia, ENSO was correlated with rainfall in that location [18]. This study shows that the rate of D75 in the province of South Sulawesi for a period of 2009 to 2016 is only significantly influenced by MJO and IOD, while ENSO does not have a significant effect. It can happen when ENSO merges concurrently with MJO or IOD or even both. Jones et al. [19] stated that MJO in the active phase led to increased extreme rainfall, where MJO generally tends to be most active during the ENSO neutral phase and experiences

a resting phase when ENSO strengthens. Also, IOD reduces the impact of ENSO, while merging at the same time [20]. MJO is stronger during negative IOD compared with positive IOD [21]. When IOD is negative, MJO increases the probability of the occurrence of high extreme rainfall. When IOD is positive, the modulation of the wet days by MJO becomes weaker.

## 7. Conclusion

This study shows that for the period of 2009 to 2016, IOD and MJO are associated with the rate of the number of extreme rainfall days. When there is a negative IOD, the incidence of the number of extreme rainfall days tends to increase. MJO in the active phase affects the rate of high extreme rainfall events at the location it passes. The ENSO does not have a significant effect on the rate of D75 events. The random effect of spatial shows a significant effect, which means that the rate of the number of extreme rainfall days in the area of the province of South Sulawesi affects the rate of occurrence in neighboring locations.

**Acknowledgement**

We thank our anonymous reviewers for their valuable advice which has improved the quality of this paper. The authors acknowledge the Ministry of Research and Technology/National Agency for Research and Innovation (RISTEK-BRIN), Indonesia for funding this research via Grant PDUPT Hasanuddin University in 2020 with grant number 1516/UN4.22/PT.01.03/2020. We would like to gratefully acknowledge Global Satellite Mapping of Precipitation, for providing the data set used in this study.

## References

[1] The Intergovernmental Panel on Climate Change (IPCC): *Managing the Risk of Extreme Events and Disasters to Advance Climate Change Adaptation*. Cambridge University Press, Cambridge, UK and New York, USA, 2012.

[2] Coles S.: *An Introduction to Statistical Modeling of Extreme Values*. Springer, Bristol 2001.

[3] Zhang Q., Li J., Singh V.P.: *Application of Archimedean copulas in the analysis of the precipitation extremes: effects of precipitation changes*. Theoretical and Applied Climatology, vol. 107, 2011, pp. 255–264.

[4] Hendon H.H.: *Indonesian Rainfall Variability: Impacts of ENSO and Local Air–Sea Interaction.* Journal of Climate, vol. 16, issue 11, 2003, pp. 1775–1790.

[5] Nur'utami M.N., Hidayat R.: *Influences of IOD and ENSO to Indonesian Rainfall Variability: Role of Atmosphere-ocean Interaction in the Indo-pacific Sector*. Procedia Environmental Sciences, vol. 33, 2016, pp. 196–203.

[6] Hidayat R.: *Modulation of Indonesian Rainfall Variability by the Madden-Julian Oscillation*. Procedia Environmental Sciences, vol. 33, 2016, pp. 167–177.
[7] Keim B.D., Cruise F.J.: *A Technique to Measure Trends in the Frequency of Discrete Random Events*. Journal of Climate, vol. 11, 1998, pp. 848–855.
[8] Wong H.L., Hsieh S.H., Tu Y.H.: *Application of Non-Homogeneous Poisson Process Modeling to Containership Arrival Rate*. [in:] *2009 Fourth International Conference on Innovative Computing, Information and Control: ICICIC 2009; Kaohsiung, Taiwan, 7–9 December 2009*, Institute of Electrical and Electronics Engineers, 2009, pp. 849–854.
[9] Achcar J.A., Rodrigues E.R., Paulino C.D., Soares P.: *Non-homogeneous Poisson models with a change-point: an application to ozone peaks in Mexico city*. Environmental and Ecological Statistics, vol. 17, 2010, pp. 521–541.
[10] Sirangelo B., Ferrari E., de Luca D.: *Occurrence analysis of daily rain-falls through non-homogeneous poissonian processes*. Natural Hazards and Earth System Sciences, vol. 11, 2011, pp. 1657–1668.
[11] Mondal A., Mujumdar P.P.: *Modeling non-stationarity in intensity, duration and frequency of extreme rainfall over India.* Journal of Hydrology, vol. 521, 2015, pp. 217–231.
[12] Huang X., Grace P., Hu W., Rowlings D., Mengersen K.: *Spatial prediction of $N_2O$ emissions in pasture: a Bayesian model averaging analysis*. PLoS One, vol. 8(6), 2013, e65039.
[13] Rusworth A., Lee D., Mitchell R.: *A spatio-temporal model for estimating the long-term effects of air pollution on respiratory hospital admissions in Greater London*. Spatial and Spatio-temporal Epidemiology, vol. 10, 2014, pp. 29–38.
[14] Sharkey P., Winter H.C.: *A Bayesian spatial hierarchical model for extreme precipitation in Great Britain*. 2017, arXiv:1710.02091v1.
[15] Marco M., Gracia E., López-Quílez A.: *Linking Neighborhood Characteristics and Drug-Related Police Interventions: A Bayesian Spatial Analysis*. ISPRS International Journal of Geo-Information, vol. 6(3), 2017, 65. https://doi.org/10.3390/ijgi6030065.
[16] Banerjee S., Carlin B., Gelfand A.: *Hierarchical Modeling and Analysis for Spatial Data*. Monographs on Statistics and Applied Probability, 101, Chapman and Hall/CRC Press, New York 2004.
[17] Deni O.L., Edy S., Sabaruddin S., Iskhaq I.: *Respective Influences of Indian Ocean Dipole and El Niño-Southern Oscillation on Indonesian Precipitation*. Journal of Mathematical and Fundamental Sciences, vol. 50, no. 3, 2018, pp. 257–272.
[18] Lee H.S.: *General Rainfall Patterns in Indonesia and the Potential Impacts of Local Seas on Rainfall Intensity*. Water, vol. 7(4), 2015, pp. 1751–1768.
[19] Jones Ch., Waliser D.E., Lau K.M., Stern W.: *Global occurrences of extreme precipitation and the Madden–Julian Oscillation: observations and predictability*. Journal of Climate, vol. 17(23), 2004, pp. 4575–4589.

[20] Ashok K., Guan Z., Saji N.H., Yamagata T.: *Individual and Combined Influences of ENSO and the Indian Ocean Dipole on the Indian Summer Monsoon*. Journal of Climate, vol. 17, 2004, pp. 3141–3155.

[21] Pourasghar F., Oliver E.C.J., Holbrook N.J.: *Modulation of wet-season rainfall over Iran by the Madden–Julian Oscillation, Indian Ocean Dipole and El Niño–Southern Oscillation*. International Journal of Climatology, vol. 39, 2019, pp. 1–12. https://doi.org/10.1002/joc.6057.

GEOMATICS AND ENVIRONMENTAL ENGINEERING • Volume 15 • Number 2 • 2021

https://doi.org/10.7494/geom.2021.15.2.17

Monika Biryło[1], Zofia Rzepecka[2]

# An Analysis of Total Water Storage Changes Obtained from GRACE FO Observations over the Venezia Islands Area Supported with Additional Data

**Abstract:** The Venezia Islands are a very special area from the hydrological point of view due to its water mass changes. Regular floods results in the need for the regular monitoring of water mass changes. For this purpose, a Gravity Recovery and Climate Experiment mission (GRACE) can be used as a source of data.
The aim of the paper is to compare the latest results of the new GRACE FO observations. The comparisons were carried out all over Venezia Island using the L3 level, RL06 release data obtained with spherical harmonics degree and order extension of up to 120, by the three most important computational centres: JPL, GFZ, CSR. Results are compared to an average month values of precipitation and evapotranspiration and tide gauge data in the nearby area.
Based on the research, no dependence between TWS and evapotranspiration and evapotranspiration change were found

**Keywords:** GRACE FO, total water storage, precipitation, evapotranspiration, tide gauges

Received: 24 August 2020; accepted: 2 February 2021



[1] University of Warmia and Mazury in Olsztyn, Department of Geodesy and Civil Engineering, Olsztyn, Poland, email: monika.sienkiewicz@uwm.edu.pl
ORCID: https://orcid.org/0000-0002-8006-288X

[2] University of Warmia and Mazury in Olsztyn, Department of Geodesy and Civil Engineering, Olsztyn, Poland, email: zofia.rzepecka@uwm.edu.pl
ORCID ID: https://orcid.org/0000-0002-6570-9032

## 1. Introduction

The research focuses on the analysis of the total water storage determined on the basis of the new GRACE FO (Gravity Recovery and Climate Experiment Follow-On) observation and comparing it with precipitation and evapotranspiration from the MERRA 2 model (The Second Modern-Era Retrospective analysis for Research and Applications), and then with tide gauge data. The research undertaken in the paper is to look for a possible relation between climatic parameters and TWS (total water storage). The research was carried out for the time span June 2018 – December 2019 for the area of the Venezia Islands. Different ways of processing were taken into consideration (traditional filtering and the newest mascon-solution). Having analysed and processed the values of monthly precipitation and evapotranspiration, an atmospheric budget was also estimated.

In the study TWS is analysed. Total water storage (TWS) is the sum of all water mass variations on land, atmosphere and in the soil; so, the sum of snow water equivalent, surface water, soil moisture and groundwater [1, 2]. TWS was and is used in many applications, like computing TWS for big river basins, like e.g. the Amazon or Mekong [3], for the improvement of hydrological models [4], correct assimilation model outputs [5], computing water budget in combination with other products [6], estimating groundwater storage [1, 7], finding TWS relationship with climate variability and human activities [8].

Precipitation (P) can be described as water droplets falling to the surface and can be in different forms: rain, sleet, snow and hail. It is usually measured as the rain volume which falls to the Earth per area unit per time unit. The rainfall rate can be used in many applications, such as water and energy cycle assessment, environmental and agricultural issues, weather forecasting, monitoring climate change, hydrological applications and natural disaster management [9, 10].

Evapotranspiration (EV) is the total value of evaporation and plant transpiration. It can be understood as water movement to the air from different sources on Earth (like soil, rivers, oceans, plants, etc.). In atmospheric models, the rate of evapotranspiration is presented as the volume of water lost from a surface unit per time unit. Evapotranspiration is used in applications such as water and atmospheric cycles evaluation, as well as weather and climate prediction models [11, 12].

The aim of the GRACE FO mission (Gravity Recovery and Climate Experiment Follow On) is to track the Earth's water movement in a global sense. It started on May 2018. GRACE satellites move on a quasi-polar orbit (89° inclination) at an altitude of about 500 km. This allows for a global coverage of continental surfaces [2]. Observations consist of monitoring changes in the following: ice and glaciers, groundwater, the amount of water in basins, and changes in sea level. Such measurements provide a unique, precise, and global view of the Earth's climate. The on-ground GRACE Science Data System releases monthly solutions by three processing centres that use their own specific algorithm to obtain Level 2 data:

GFZ, CSR and JPL. Data is provided on three levels, with the first level being raw data. The typical user usually analyses and process data on the second level, and in a somewhat different way for every centre [13].

For the purpose of obtaining the vales of monthly changes of precipitation and evapotranspiration data, MERRA 2 model outputs were obtained. The Modern-Era Retrospective analysis for Research and Applications (MERR2) is a NASA (National Aeronautics and Space Administration) atmospheric reanalysis model, determined for global, accurate spatial and time resolution releases of meteorological units. Outputs are based on satellite and terrestrial observations combined with GCM (General Circulation Model) simulations [14]. The data is available in grid form, at the 0.625° longitude × 0.5° latitude resolution [15].

Tide gauges were obtained from a website of the Permanent Service for Mean Sea Level (PSMSL) [16], a service providing global data of mean sea level changes.

## 2. Case Study – Venezia

The study focuses on the Venezia Islands, one of the most interesting hydrological systems in southern Europe due to its island character and interesting hydrological situation. The analysed basin drains 60,500 km². This study analyses water mass variations for both the land and sea area.

Venezia Islands are the biggest lagoon in the area of the Mediterranean (Figs. 1, 2).


**Fig. 1.** Research location

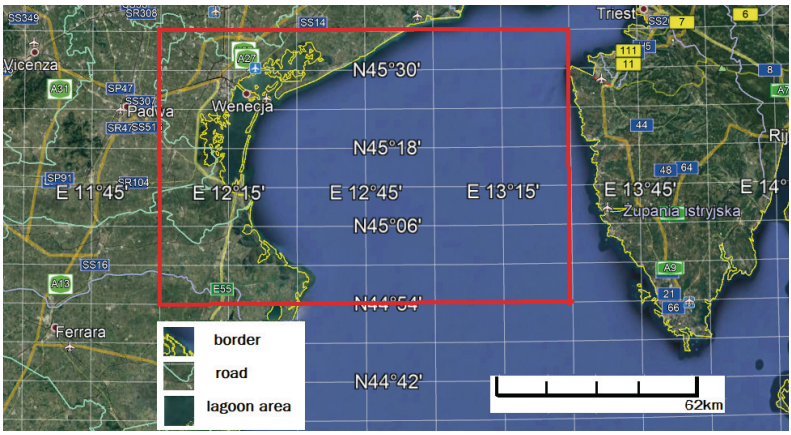


**Fig. 2.** GRACe grids used in the computation

The area can be characterized as a microtidal regime. According to the atmospheric conditions, especially the occurrence of the sirocco (strong winds from the south) and storms caused by a low atmospheric pressure should be emphasized. Such conditions influence the significant increase of the maximum water level [17–19].

## 3. Methods

In the paper a total water storage was determined and then compared to meteorological and tide gauge data. Thanks to the GRACE mission, we are able monitor processes that involve mass redistribution [20]. Because of this fact the total water storage changes from GRACE can then become a good basis for water and energetic budget analysis.

### 3.1. Total Water Storage Determination Using Spherical Harmonics

In the paper two ways of determining TWA are presented. The first is to compute TWS from the spherical harmonics coefficient extension with a degree and order of 120. As the raw data suffers from data leakage and needs a destriping process, Gauss filtering of a radius 300 km was introduced.

TWS was determined with the formula [21]:

$$\Delta TWS = \frac{a\rho_{ave}}{\rho_{water}} \sum_{t=0}^{\infty} \sum_{m=0}^{l} \frac{2l+1}{1+k_l} \overline{P_{lm}} \cos\theta \left( \Delta \overline{C_{lm}} \cos m\varphi + \overline{S_{lm}} \sin m\varphi \right),$$

where: $\theta$ and $\varphi$ are colatitude and longitude, $a$ is the radius of the Earth equal 6 378 136.300 m, $\rho_{ave}$ is the average density of the Earth equal 5517 kg/m$^3$, $\rho_{water}$ is the density of water equal 1000 kg/m$^3$, $k_l$ is the load Love number, and $\overline{P_{lm}}$ is the fully normalized associated Legendre functions.

To define the isotropic Gauss a radius $r$, and consists of the application of a weight, $W_{lm}$, added to the elements of the spherical harmonics coefficient $S_{lm}$ and $C_{lm}$. So, with a filtering weight, TWS changes estimated as [22, 23]:

$$\Delta TWS = \frac{a\rho_{ave}}{\rho_{water}} \sum_{t=0}^{\infty} \sum_{m=0}^{l} \frac{2l+1}{1+k_l} W_{lm} \overline{P_{lm}} \cos\theta \left( \Delta \overline{C_{lm}} \cos m\varphi + \overline{S_{lm}} \sin m\varphi \right).$$

The radius $r$ of the Gauss filter only defines the filter approximately, its purpose is to fix the spatial resolution of the filtered grids.

### 3.2. Total Water Storage Determination Using Mascons

On the other hand, mascon processing of GRACE observations was used. Mascons (mass concentrations blocks) are some kind of mass concentration beneath the surface of a planet and are the cause of changes in the gravitational field. Mascon parameters are used to obtain geographical corrections for the mean global gravity field. Each of the parameters represents the excess or deficit of surface mass for a specific area and a designated time period. The excess or deficit of surface mass determined for a specific area is represented as a uniform layer of mass, which is expressed in meters of total water storage in that region. In other words, mascons represent the distribution of surface mass as spatial and temporal functions [24].

### 3.3. Steps of Research

All in all, based on GRACE observations, TWS variations are computed using two techniques (Fig. 3).

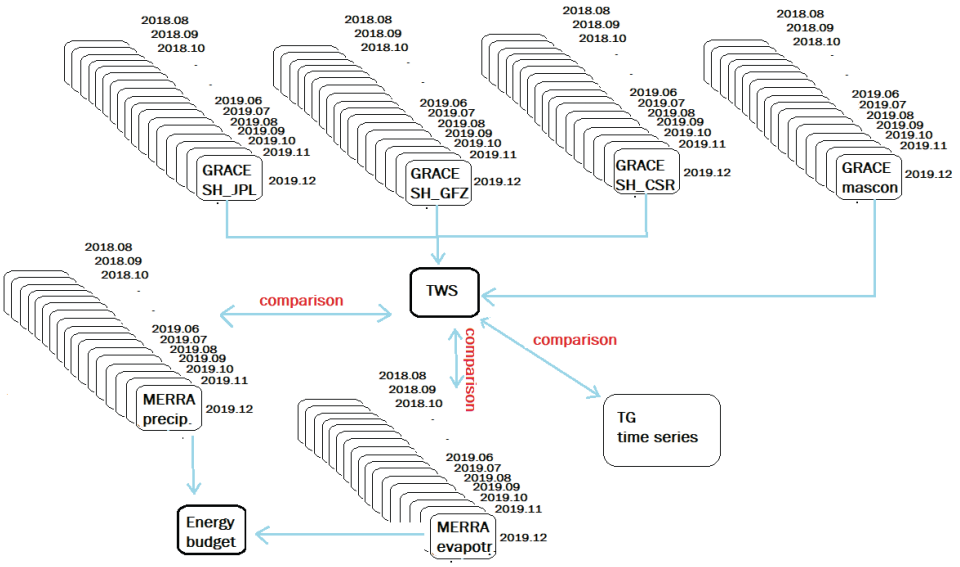


**Fig. 3.** Flowchart of GRACE observations processing

Next, TWS changes are analysed in terms of looking for the causes of changes. Precipitation and evapotranspiration from the satellite model, and sea level changes due to tide gauges will be taken into account. Due to the marine climatic zone, the relatively flat surface (a small part of the researched area is land, which can be classified as flat), canopy and surface topography influence will not be considered.

## 4. Results and Discussion

From a website [25] the observations concerning total water storage were downloaded. Three types of postprocessing were taken into calculation – Release Note 06 computed in the computation centres JPL – Jet Propulsion Laboratory [26] GFZ – German Research Centre for Geosciences (GeoForschungsZentrum) [27] and CSR – Center for Space Research at University of Texas, Austin [28]. Gridded surface TWS variations over the Venezia Island area were derived from spherical harmonic coefficients that represent the Earth's mean gravity field estimations during the specified one-month timespan. Obtained results are a good approximation of the full magnitude of land hydrology and land ice. For the purpose of raw data filtering, a Gauss filter with a 300 km radius was used [29].

GRACE data with a spatial resolution of approximately 100 km is characterized with a significant noise ratio (the noise increases with degrees of the spherical harmonic decomposition striving for a higher spatial resolution). The aim of the three mentioned centres is to reduce noise by applying smoothing filters. In fact, smoothing filters cause the smoothing of the amplitude of the water mass variations. Moreover, TWS also suffers leakage effects [3, 30]. D. Long et al. [31] made research on 60 river basins and noticed more disparities in TWS trend for medium basins that are less than 200,000 km$^2$. Based on the research it can be said that more differences in TWS are more likely to be noticed for medium and small watersheds. The research area covers a small zone, so three solutions were considered (Fig. 4).

Correlation coefficients were computed between all the time series, the results are as follows:

- GFZ/JPL: 0.972,
- GFZ/CSR: 0.975,
- JPL/CSR: 0.983.

Analysing the values of TWS over the Venezia Islands led the authors to notice that the smallest values of TWS change were achieved in late-autumn period (−13 cm in October 2018 and −15 cm in October 2019). In summer, the TWS change is almost zero (0.6 cm in June 2019). Analysing old TWS data measured by the GRACE mission from 2002 to 2017 let us notice that such a tendency is stable over the years, with values of about 14 cm in autumn and about 0 cm in the beginning of the summer [32].

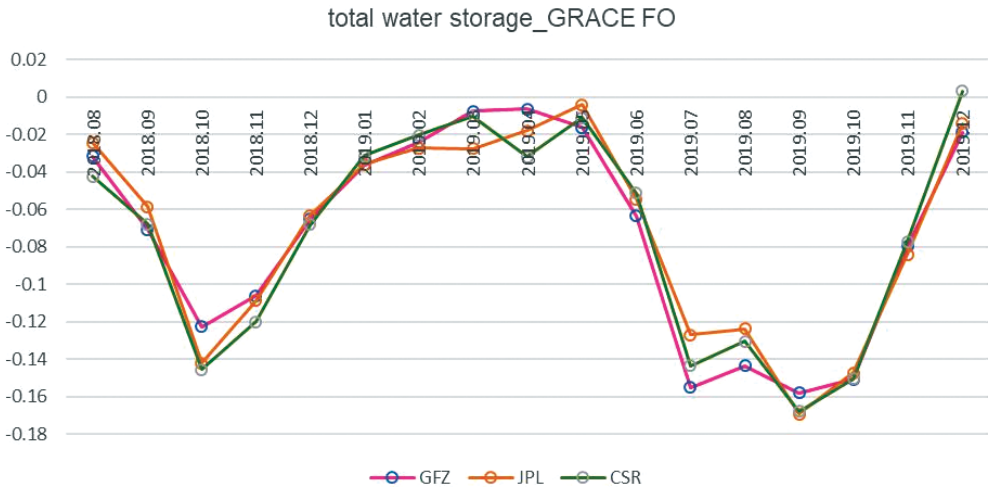


**Fig. 4.** Total water storage changes – time series for GFZ, JPL and CSR solution filtered with Gauss, 300 km radius, for the whole researched area of the Venezia Islands, unit: metres

According to [13], it is recommended to use a simple arithmetic mean of the JPL, CSR, GFZ fields. Such an approach seems to be the most effective in cases of reducing the noise in the solutions. The differences between solutions of JPL, GFZ, and CSR releases are rather small, and are dependent on the error bounds of the GRACE solution itself [13]. Because the correlation coefficient is more than 0.9, time series filtered with Gauss 300 km were averaged. In the next step of the research, it was checked if the averaged filtered solutions correspond to the newest mascons solutions.

In comparison to the filtering solution, the aim of mascons is to parameterize the Earth's gravity field with mass concentration functions. Such a solution causes the decrease of leakage [33]. In the paper, the mascon solution computed by the JPL centre (0.5°× 0.5° grid, RL06 M.MSCNv01 dataset with Coastal Resolution Improvement Filtering [34]) was used (Fig. 5).

The correlation coefficient between the mascon solution and the average time series of filtered TWS values is very high (0.995). It can be said that for the area of the Venezia Islands, both solutions can be used interchangeably.

Using the web-service [35], two sets of MERRA 2 outputs were obtained in a one-month time resolution: precipitation and evapotranspiration. The data was averaged for every month over the researched area. Analysing the evapotranspiration time series, a smooth regular line is noticed. The Venezia Islands have a moderately warm climate, and annual amplitudes of the temperature are rather small. Figure 6 reflects the climate. In summer, when more sun radiation and longer days are noted, values of evapotranspiration are on the level from 3.5 to 5 e–5 kg/m$^2$/s. In winter months, evapotranspiration is about 1.5 e–5 kg/m$^2$/s. Precipitation rate over year is

more irregular, during the analysed period the highest value is noticed in November 2019 (10 e–5 kg/m$^2$/s). It needs to be mentioned that this was the time of a very dangerous flood that occurred in Venezia Lagoon (caused by an unexpectedly huge tide) while a year before, in November 2018, the value of precipitation was only 4.2 e–5 kg/m$^2$/s.

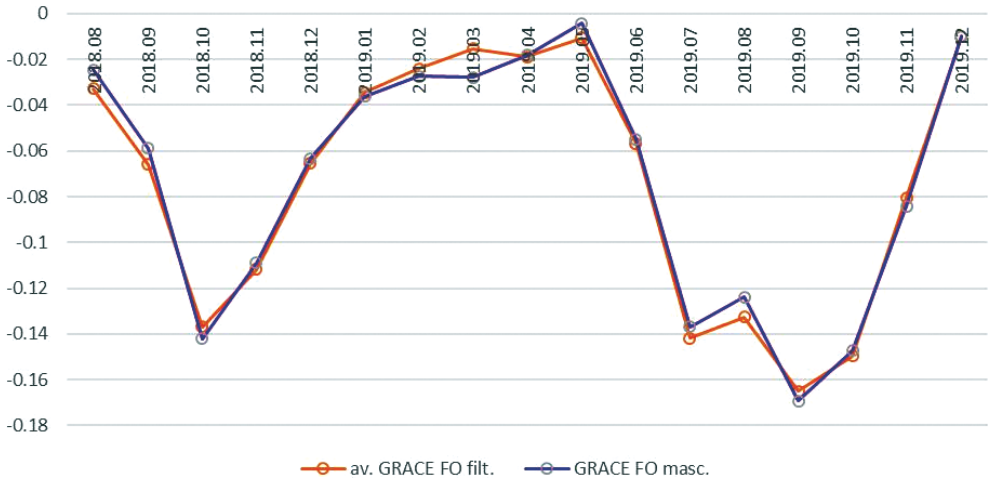


**Fig. 5.** Total water storage changes – time series for averaged GFZ, JPL and CSR solution filtered with Gauss, 300 km radius, and time series for mascon solution, for the whole researched area of the Venezia Islands, unit: metres

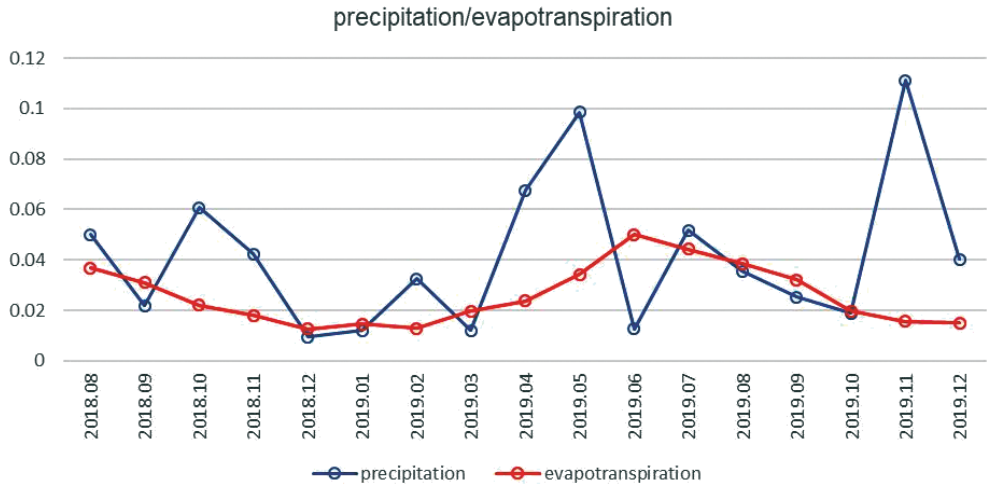


**Fig. 6.** Precipitation and evapotranspiration outputs from the MERRA 2 model, for the entire research area of the Venezia Islands, unit: kg/m$^2$/s

The values of precipitation and evapotranspiration were recomputed into metres for the purpose of performing a comparison between the TWS and MERRA 2 outputs (Fig. 7). It can be said that there is no relation between evapotranspiration and TWS as the value and amplitude of an evapotranspiration change is insignificantly small in comparison with TWS. Analysing the relation between precipitation change and TWS change, much higher values are noticed according to precipitation. The precipitation rate seems to have very little influence on TWS variations. As Venezia is characterized with an island geographical location, it seems that tides have such a huge influence that determines most of the monthly TWS values. No significant linear relationship has also been demonstrated in Figures 8 and 9, where a scatterplot of correlation between TWS and precipitation, together with TWS and evapotranspiration, are presented.

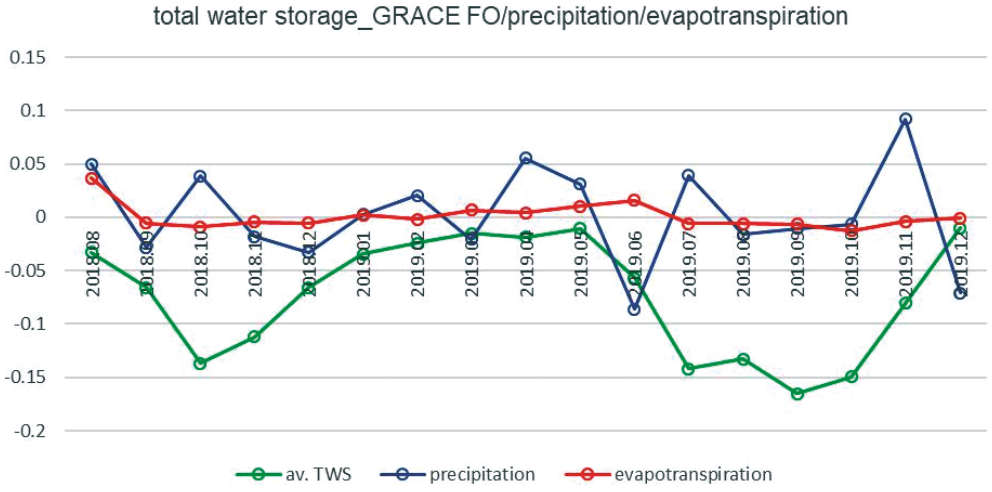


**Fig. 7.** Comparison between average total water storage changes, precipitation and evapotranspiration, for the whole researched area of the Venezia Islands, unit: metres

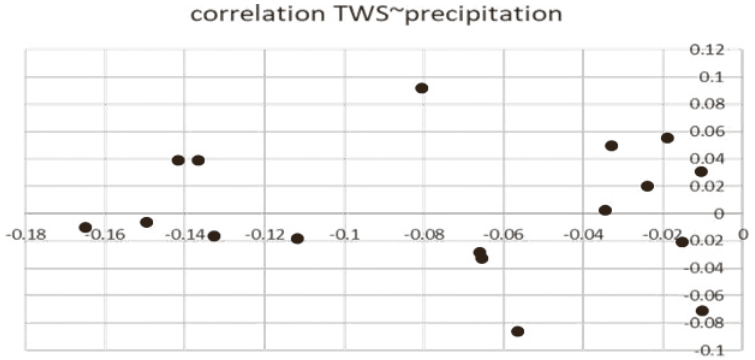


**Fig. 8.** Relation between TWS and precipitation, for the area of the Venezia Islands, unit: metres

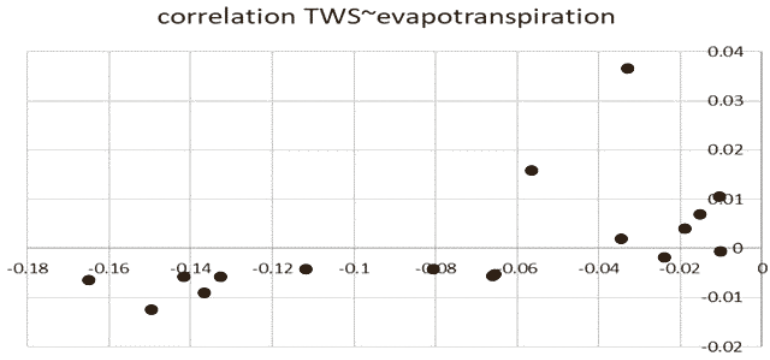


**Fig. 9.** Relation between TWS and evapotranspiration, for the area of the Venezia Islands, unit: metres

In the near surroundings of Venezia, four mareograph stations are to be found:
– VENEZIA ARSENALE (45.417; 12.350),
– VENEZIA II (45.418; 12.427),
– VENEZIA – S.STEFANO (45.417; 12.333),
– VENEZIA – PUNTA DELLA SALUTE (45.433; 12.333).

For the purpose of the research of tide gauge changes, a mareograph from VENEZIA II was taken, having the most up to date data. The comparison between TWS and mean sea level changes is presented in Figure 10.

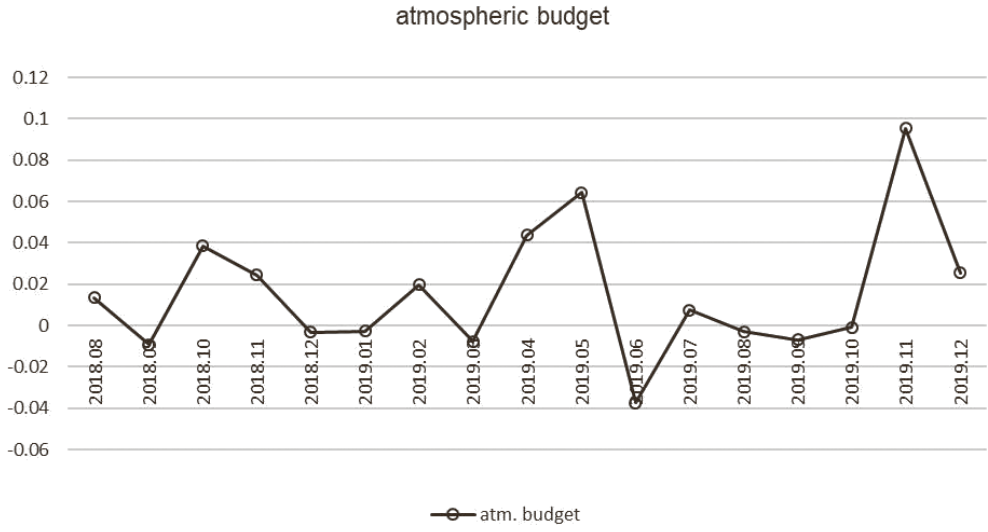


**Fig. 10.** Relation between TWS and tide gauges changes, for the whole researched area of the Venezia Islands, unit: metres

This can prove that any change of mean sea level change is quickly reflected in TWS changes. Values from tide gauge measurements are higher that TWS changes, bringing the conclusion that some big run off is expected in a region up to about 0.25 metres change) yet it can be noticed that phases of changes are the same. A rise of both TWS and tide gauge data change was observed for the period December 2018 – June 2019, then during a period July 2019 – November 2019 negative values are observed. It would be interesting to extend the time series of measurement for the purpose of looking for seasonal repeat.

The last part of the research was to compute the availability of fresh water in the area. Having the values of precipitation and evapotranspiration, an atmospheric budget over the region was also computed (Fig. 11). Freshwater availability monitoring and understanding is of immense importance, especially in assessing the social, economic, and environmental impacts of climate change. Estimation of the approximate freshwater availability can be computed as the difference (P–E) between precipitation (P) and evapotranspiration (E). Such an approach is widely practiced because of its simplicity [36–38].

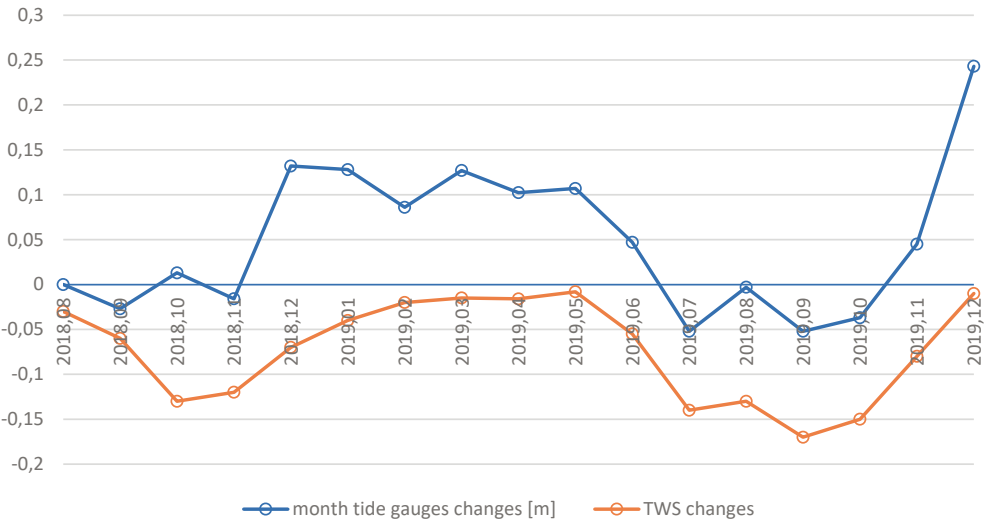


**Fig. 11.** Atmospheric budget for the area of the Venezia Islands, unit: metres

In the area of the Venezia Islands, an atmospheric budget in half of the researched months gained a so-called normal value (approx. 0). This means that precipitation and evapotranspiration chance is balanced. The only below normal value was noticed in June 2019 (−4 cm). The highest values of the atmospheric budget, an above normal budget, were noticed in November 2019 (9 cm), May 2019 (6.5 cm) and in October 2018 (4 cm).

## 5. Conclusions

The aim of the paper was to check for dependencies between total water storage change and precipitation and evapotranspiration change over the area of the Venezia Islands. Based on the research, a few conclusions were drawn.

1. No dependence between TWS and evapotranspiration and evapotranspiration change was found. The major impact on TWS change must be by the influence of tides.
2. There is a high correlation between all analysed filtered solutions (GFZ, JPL and CSR) and between averaged filtered solution and the newest mascon solution over the Venezia Islands. Both solutions can be used interchangeably.
3. A similar phase of changes can be observed when comparing TWS changes and tide gauge data changes.
4. Atmospheric budget analyses reveal normal or above normal values which is a good prognostic of the availability of fresh water.

## References

[1] Chen J., Famiglietti J.S., Scanlon B.R., Rodell M.: *Groundwater storage changes: present status from GRACE observations*. Surveys in Geophysics, vol. 37(2), 2016, pp. 397–417.

[2] Biancamaria S., Mballo M., Le Moigne P., Pérez S.J.M., Espitalier-Noël G., Grusson Y., Cakir R., Häfliger V., Barathieu F., Trasmonte M., Boone A., Martin E., Sauvage S.: *Total water storage variability from GRACE mission and hydrological models for a 50,000 km$^2$ temperate watershed: the Garonne River basin (France)*. Journal of Hydrology: Regional Studies, vol. 24, 2019, 100609.

[3] Wouters B., Bonin J.A., Chambers D.P., Riva R.E.M., Sasgen I., Wahr J.: *GRACE, time-varying gravity, Earth system dynamics and climate change*. Reports on Progress in Physics, vol. 77, no. 11, 2014, 116801.

[4] Niu G.Y., Yang Z.L.: *Assessing a land surface model's improvements with GRACE estimates*. Geophysical Research Letters, vol. 3, 2006, L07401.

[5] Zaitchik B.F., Rodell M., Reichle R.H.: *Assimilation of GRACE terrestrial water storage data into a land surface model: results for the Mississippi River basin*. Journal of Hydrometeorology, vol. 9(3), 2008, pp. 535–548.

[6] Gao Y., Tang Q., Ferguson C.R., Wood E.F., Lettenmaier D.P.: *Estimating the water budget of major US river basins via remote sensing*. International Journal of Remote Sensing, vol. 31, no. 14, 2010, pp. 3955–3978.

[7] Śliwińska J., Birylo M., Rzpecka Z., Nastula J.: *Analysis of groundwater and total water storage changes in Poland using GRACE observations, in-situ data, and various assimilation and climate models*. Remote Sensing, vol. 11, 2019, 2949.

[8] Rodell M., Famiglietti J.S., Wiese D.N., Reager J.T., Beaudoing H.K., Landerer F.W., Lo M.H.: *Emerging trends in global freshwater availability*. Nature, vol. 557, 2008, pp. 651–659.

[9] Saha G.C.: *Climate Change Induced Precipitation Effects on Water Resources in the Peace Region of British Columbia, Canada*. Climate, vol. 3(2), 2015, pp. 264–282.

[10] GES DISC: *Giovanni Measurement Definitions: Precipitation*. https://disc.gsfc.nasa.gov/information/glossary?keywords=giovanni%20measurements&title=Giovanni%20Measurement%20Definitions:%20Precipitation [access: 10.02.2020].

[11] Moorhead J.E., Marek G.W., Gowda P.H., Lin X., Colaizzi P.D., Evet S.R., Kutikoff S.: *Evaluation of Evapotranspiration from Eddy Covariance Using Large Weighing Lysimeters*. Agronomy, vol. 9, no. 2, 2019, 99.

[12] LDAS – Land Data Assimilation System. http://ldas.gsfc.nasa.gov/faq/#NLDAS_evap [10.02.2020].

[13] Sakumura C., Bettadpur S., Bruinsma S.: *Ensemble prediction and intercomparison analysis of GRACE time-variable gravity field models*. Geophysical Research Letters, vol. 41(5), 2014, pp. 1389–1397.

[14] Wargan K., Labow G., Frith S., Pawson S., Livesey N., Partyka G.: *Evaluation of the Ozone Fields in NASA's MERRA-2 Reanalysis*. Journal of Climate, vol. 30(8), 2017, pp. 2961–2988.

[15] Rienecker M.M., Suarez M.J., Gelaro R., Todling R., Bacmeister J., Liu E., Bosilovich M.G., Schubert S.D., Takacs L., Kim G.K., Bloom S., Chen J., Collins D., Conaty A., da Silva A., Gu W., Joiner J., Koster R.D., Lucchesi R., Molod A., Owens T., Pawson S., Pegion P., Redder C.R., Reichle R., Robertson F.R., Ruddick A.G., Sienkiewicz M., Woollen J.: *MERRA: NASA's Modern-Era Retrospective Analysis for Research and Applications*. Journal of Climate, vol. 24(14), 2011, pp. 3624–3648.

[16] PSMSL – Permanent Service for Mean Sea Level. https://www.psmsl.org/ [access: 18.02.2020].

[17] Molinaroli M., Guerzoni S., Sarretta A., Cucco A., Umgiesser G.: *Links between hydrology and sedimentology in the Lagoon of Venice, Italy*. Journal of Marine Systems, vol. 68(3–4), 2007, pp. 303–317.

[18] Pirazzoli P.A.: *Possible defences against a sea level rise in the Venice area, Italy*. Journal of Coastal Research, vol. 7, no. 1, 1991, pp. 231–248.

[19] Canestrelli P., Mandich M., Pirazzoli P.A., Tomasin A.: *Wind, depression and seiches: tidal perturbations in Venice (1951–2000)*. Technical Report, Comune di Venezia, Centro Previsioni e Segnalazioni Maree, Venice, Italy, 2001.

[20] Wahr J., Molenaar M., Bryan F.: *Time variability of the Earth gravity firld: hydrological aand oceanic effects and their possible detection using GRACE*. Journal of Geophysical Research – Solid Earth, vol. 103(B12), 1998, pp. 30205–30229.

[21] Hassan A., Jin S.: *Water cycle and climate signals in Africa observed by satellite gravimetry*. IOP Conference Series: Earth and Environmental Science, vol. 17, 2014, 012149.
[22] Jekeli C.: *Alternative Methods to Smooth the Earth's Gravity Field*. Geodetic and Geoinformation Science Department of Civil and Environmental Engineering and Geodetic Science, The Ohio State University, Columbus, Ohio 1981.
[23] Swenson S., Wahr J.: *Methods for inferring regional surface mass anomalies from Gravity Recovery and Climate Experiment (GRACE) measurements of time-variable gravity*. Journal of Geophysical Research – Solid Earth, vol. 107(B9), 2002, pp. ETG 3-1–ETG 3-13.
[24] Rowlands D., Luthcke S., McCarthy J., Klosko S., Chinn D., Lemoine F., Boy J.-P., Sabaka T.: *Global mass flux solutions from GRACE: A comparison of parameter estimation strategies – Mass concentrations versus stokes coefficients*. Journal of Geophysical Research – Solid Earth, vol. 115(B1), 2010, B01403.
[25] GRACE-FO – NASA. https://gracefo.jpl.nasa.gov/ [access: 3.02.2020].
[26] JPL GRACE Tellus – NASA. https://grace.jpl.nasa.gov/ [access: 8.02.2020].
[27] GRACE-FO Geopotential GSM Coefficients GFZ RL06. http://dataservices.gfz-potsdam.de/gracefo/showshort.php?id=escidoc:4289898 [access: 8.02.2020].
[28] PO.DAAC – NASA. https://podaac.jpl.nasa.gov/ [access: 8.02.2020].
[29] Swenson S., Wahr J.: *Post-processing removal of correlated errors in GRACE data*. Geophysical Research Letters, vol. 33(8), 2006, L08402.
[30] Longuevergne L., Scanlon B.R., Wilson C.R.: *GRACE Hydrological estimates for small basins: Evaluating processing approaches on the High Plains Aquifer, USA*. Water Resources Research, vol. 46(11), 2010, W11517.
[31] Long D., Pan Y., Zhou J., Chen Y., Hou X., Hong Y., Scanlon B.R., Longuevergne L.: *Global analysis of spatiotemporal variability in merged total water storage changes using multiple GRACE products and global hydrological models*. Remote Sensing of Environment, vol. 192, 2017, pp. 198–216.
[32] The GRACE Plotter. http://thegraceplotter.com/ [access: 21.02.2020].
[33] Scanlon B.R., Zhang Z., Save H., Wiese D.N., Landerer F.W., Long D., Longuevergne L., Chen J.: *Global evaluation of new GRACE mascon products for hydrologic applications*. Water Resourches Research, vol. 52(12), 2016, pp. 9412–9429.
[34] Watkins M.M., Wiese D.N., Yuan D.N., Boening C., Landerer F.W.: *Improved methods for observing Earth's time variable mass distribution with GRACE using spherical cap mascons*. JGR Solid Earth, vol. 120(4), 2015, pp. 2648–2671.
[35] NASA Giovanni. https://giovanni.gsfc.nasa.gov/giovanni/ [access: 31.01.2020].

[36] Trenberth K.E., Fasullo J.T.: *North American water and energy cycles*. Geophysical Research Letters, vol. 40, 2016, pp. 365–369.
[37] Oki T., Kanae S.: *Global hydrological cycles and world water resources*. Science, vol. 313, 2006, pp. 1068–1072.
[38] Parish E.S., Kodra E., Steinhaeuser K., Ganguly A.R.: *Estimating future global per capita water availability based on changes in climate and population*. Computers & Geosciences, vol. 42, 2012, pp. 79–86.